





Continuous-variable nonclassicality certification under coarse-grained measurement

Chan Roh ¹, Young-Do Yoon ¹, Jiyong Park ^{2,*} and Young-Sik Ra ^{1,†}

¹*Department of Physics, Korea Advanced Institute of Science and Technology, Daejeon 34141, Korea*

²*School of Basic Sciences, Hanbat National University, Daejeon 34158, Korea*



(Received 6 January 2023; revised 30 August 2023; accepted 7 September 2023; published 18 October 2023)

Coarse graining is a common imperfection of realistic quantum measurement, obstructing the direct observation of quantum features. Under highly coarse-grained measurement, we experimentally certify the continuous-variable nonclassicality of both Gaussian and non-Gaussian states. Remarkably, we find that this coarse-grained measurement outperforms the conventional fine-grained measurement for nonclassicality certification: it detects nonclassicality beyond the reach of the variance criterion, and furthermore, it exhibits stronger statistical significance than the high-order moments method. Our work demonstrates the usefulness of coarse-grained measurement by providing a reliable and efficient way of nonclassicality certification for quantum technologies.

DOI: [10.1103/PhysRevResearch.5.043057](https://doi.org/10.1103/PhysRevResearch.5.043057)

I. INTRODUCTION

A continuous-variable (CV) quantum state of light is a versatile quantum resource for quantum information technologies: quantum states encoded in the continuous field quadratures are used for quantum computing [1–6], quantum communication [7,8], and quantum metrology [9,10]. In particular, even a single-mode CV quantum state—where entanglement is absent by construction—can show quantum enhancement, e.g., in quantum parameter estimation [10,11] and quantum key distribution [12]. Furthermore, a single-mode CV quantum state (e.g., a squeezed state and a Gottesman-Kitaev-Preskill state [13]) is a basic building block to construct a large-scale entangled system [1,2,14–16]. To exploit such quantum resources in practice, it is essential to certify the nonclassicality of experimentally generated states.

A nonclassical state is defined as a state which cannot be expressed as a statistical mixture of coherent states [16]. Nonclassicality can in principle be certified by performing quantum state tomography, but it is a demanding process requiring informationally complete measurements and maximum-likelihood reconstruction [17–19]. Alternatively, measuring the variance of a single quadrature alone can detect nonclassicality [20]; however, its application is generally limited to Gaussian states. For the case of non-Gaussian states, there are methods of measuring high-order moments [21,22] or a characteristic function [23,24], but these require substantial data collection to achieve sufficient statistical significance. Even worse, under *coarse-grained measurement*, all of these methods are subject to *false-positive* certification of

nonclassicality, and thus careful considerations must be made [25–27].

Coarse graining commonly occurs in realistic quantum measurement [28], where nearby measurement outcomes are grouped together as a single bin, thereby producing the same result. It originates from a finite resolution in measurement, for example, when using image pixels [26] and quadrature [29] and photon-number [30] detection. Coarse graining, like decoherence processes, makes it hard to observe quantum features by inducing a quantum-to-classical transition [30]. In dealing with realistic situations, it is therefore necessary to establish reliable nonclassicality criteria compatible with coarse-grained measurement.

In this work, we demonstrate reliable certification of CV nonclassicality, even under considerable coarse graining in measurement. In the experiment, we show that the nonclassicality of squeezed vacuum states is directly certified under coarse-grained quadrature measurement, which is obtained only at a single quadrature (namely, the \hat{x} quadrature), i.e., no complete information is required. Interestingly, our method based on coarse-grained measurement can detect the nonclassicality of a non-Gaussian state of a phase-diffused squeezed vacuum, where the conventional variance measurement—even without coarse graining—fails to detect [20]. Furthermore, the simplicity of our method, requiring only multiplication and division of experimental data, considerably reduces the sampling error for nonclassicality certification. Consequently, the coarse-graining method rather outperforms the conventional moments method (which requires matrix decompositions [21,22]) in terms of statistical significance for nonclassicality certification; we will show that this superiority becomes more pronounced with higher squeezing and phase diffusion.

II. NONCLASSICALITY TEST

Let us start by explaining our nonclassicality test for CV quantum states. We consider a single-quadrature probability

*jiyong.park@hanbat.ac.kr
†youngsikra@gmail.com

distribution $p(x)$ of a quantum state, i.e., a marginal distribution of a Wigner function. We construct a nonclassicality test by noticing that the probability distribution of any classical state cannot exhibit a narrower structure than that of a coherent state; this is because a classical state should be expressed by a statistical sum of coherent states. Consequently, a nonclassicality test can be formulated by comparing the widths of probability distributions by a given state and a coherent state:

$$R(s) = \frac{p(s)p(-s)}{p(0)^2} e^{s^2}, \quad (1)$$

where $R < 1$ certifies nonclassicality [31]. We choose three points of $x \in (-s, 0, s)$, where $s > 0$, for the test, which is favorable for a probability distribution having a peak at the origin, but the method can be generalized to detect nonclassicality of generic quantum states [31]. In our convention, the bosonic commutation relation of quadrature operators \hat{x} and \hat{p} is given by $[\hat{x}, \hat{p}] = 2i$. The nonclassicality test in Eq. (1) can be adapted for coarse-grained measurement [31]:

$$\mathcal{R} = \frac{C_d C_{-d}}{(C_0)^2} e^{\sigma^2 d^2}. \quad (2)$$

C_m represents the count of measurement outcomes in a bin index of an integer m , which has a range of $x = [(m - 1/2)\sigma, (m + 1/2)\sigma]$ with a bin size σ . Similar to Eq. (1), three indices of $m \in (-d, 0, d)$ are chosen, where d is a positive integer. $\mathcal{R} < 1$ certifies the nonclassicality of a given state, which is applicable for both Gaussian states and non-Gaussian states, and the value of \mathcal{R} provides a lower bound on the nonclassical depth [31]. Note that \mathcal{R} can be estimated from simple multiplication and division of obtained counts C_m together with a predetermined value $e^{\sigma^2 d^2}$; the estimation error of \mathcal{R} is thus attributed to the statistics of C_m only. We call this nonclassicality test, Eq. (2), a *three-bin test*.

III. EXPERIMENT

We first experimentally demonstrate the three-bin test on squeezed vacuum states with various phase diffusions. Figure 1(a) describes the experimental setup. A mode-locked Ti:sapphire laser produces a 75-fs pulse train with a repetition rate of 80 MHz and a central wavelength of 800 nm. In the second harmonic generation (SHG), a pulse laser of 400 nm wavelength is generated, which is used for the pump of the synchronously pumped optical parametric oscillator (SPOPO). SPOPO has a free spectral range of 80 MHz to match the repetition rate of the Ti:sapphire laser, its finesse is 27.4, and it contains a 2-mm-thick BiBO crystal for type-I spontaneous parametric down-conversion. SPOPO generates squeezed light as operating below its threshold [3,32].

To measure the generated squeezed light, we employ homodyne detection (HD) shown in Fig. 1(a). A local oscillator (LO) beam, determining the mode of homodyne detection, is engineered by a pulse shaper for spectral mode matching with SPOPO [3,32]. The visibility and the clearance of the homodyne detection are 95% and 15 dB, respectively. We measure two sideband frequencies simultaneously (1 MHz and 2 MHz with a sampling rate of 100 kHz for each): the former is for obtaining a quadrature outcome x , and the latter is for phase information θ . By varying the phase θ with a piezoelectric

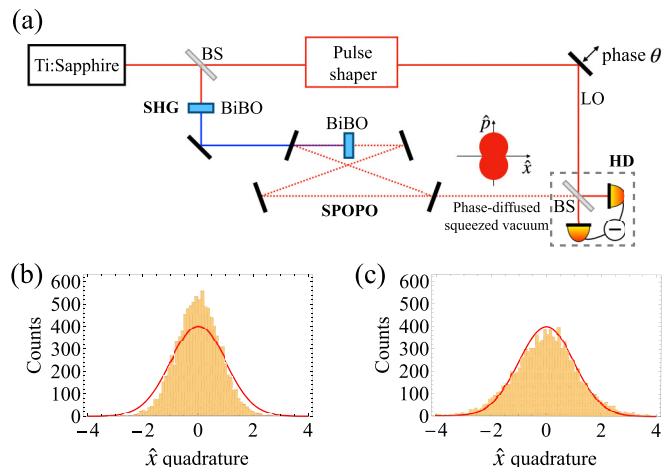


FIG. 1. (a) Experimental setup. Ti:sapphire laser produces femtosecond pulses, which are used for SHG and LO. HD measures squeezed light generated from a SPOPO. (b) Histogram of \hat{x} quadrature outcomes by a squeezed state; the variance is -2.3 ± 0.1 dB. (c) Histogram of \hat{x} quadrature outcomes by a phase-diffused squeezed state; the variance is 0.23 ± 0.07 dB, being larger than the vacuum variance. The data number is 10^4 for both (b) and (c). The red line is the vacuum distribution as a reference.

transducer, we obtain a pair of data (θ_i, x_i) for each measurement i . For choosing \hat{x} quadrature measurement, we select data within a small range of phase $\theta_i \in (-0.087, 0.087)$ rad.

Figure 1(b) shows the obtained outcomes for \hat{x} quadrature. Compared with the vacuum state, the squeezed state shows a narrower distribution, resulting in -2.3 ± 0.1 dB variance. We further characterize the amount of phase diffusion present in the generated state. For this purpose, we use the variance and the kurtosis of \hat{x} quadrature measurement and the variance of \hat{p} quadrature measurement (see Appendix A for details). The estimated phase diffusion is $\Delta_0 = 0.15 \pm 0.02$ rad, which originates from interferometer instability and the phase estimation noise. To increase the phase diffusion further, we add a random noise in a normal distribution $\epsilon \sim \mathcal{N}(0, \Delta_\epsilon^2)$ to the estimated phase θ_i :

$$(\theta_i, x_i) \rightarrow (\theta_i + \epsilon, x_i), \quad (3)$$

which increases the phase diffusion to $\Delta = \sqrt{\Delta_0^2 + \Delta_\epsilon^2}$. After adding the phase noise, we select data in the same way as before for \hat{x} quadrature measurement. We have confirmed that the resulting phase diffusion agrees well with the prediction (see Appendix A.). Figure 1(c) shows the obtained quadrature outcomes, resulting in a variance of 0.23 ± 0.07 dB (i.e., no squeezing) and a phase diffusion of 0.37 ± 0.01 rad. Note that this phase-diffused state is still nonclassical while the variance criterion ($\langle \delta \hat{x}^2 \rangle < 1$) fails to detect its nonclassicality.

Now we consider coarse-grained quadrature measurement. As the first example, we make binning on the data for the squeezed state in Fig. 1(b). The result is shown in Fig. 2(a), where the bin size σ is 1. The three-bin test with $d = 1$ detects the nonclassicality of the state under coarse-grained measurement, showing $\mathcal{R} = 0.60 \pm 0.04 < 1$. Next, we investigate the phase-diffused squeezed state in Fig. 1(c), where neither variance nor Wigner function negativity methods can detect its

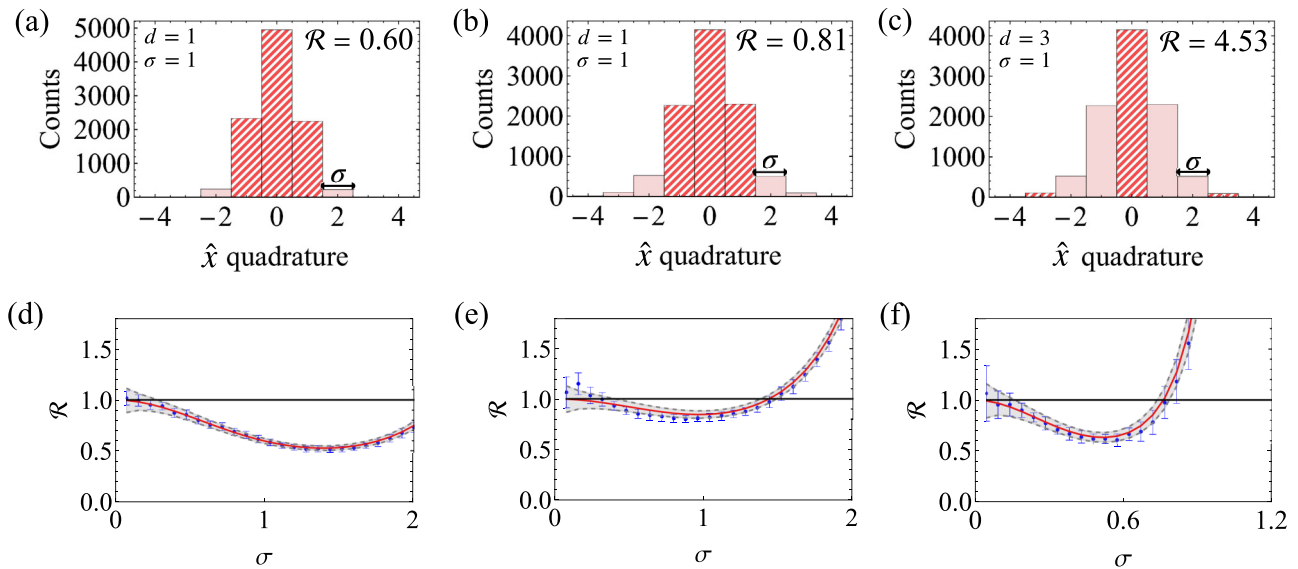


FIG. 2. Nonclassicality certification with coarse-grained quadrature measurement. Quadrature outcomes (total number: 10^4) are coarse grained with a bin size σ of one: (a) the squeezed state in Fig. 1(b); (b) and (c) the phase-diffused state in Fig. 1(c). For the nonclassicality test using Eq. (2), the three hatched bins are selected [$d = 1$ for (a) and (b), and $d = 3$ for (c)]. (d)–(f) Effect of the bin size (i.e., the coarse-graining level) on nonclassicality certification for (a)–(c), respectively. Blue dots are experimental data with error bars of one standard deviation. To obtain the statistics, we use the bootstrap method by sampling 10^4 data from the total 4×10^4 experimental data. Red lines are theoretical curves, where the shaded areas represent statistical errors by considering a finite data number (10^4). Black horizontal lines are the thresholds for nonclassicality certification (nonclassical if $\mathcal{R} < 1$).

nonclassicality. Figure 2(b) shows the result of coarse graining with $\sigma = 1$. By conducting the three-bin test, we again find a clear evidence of nonclassicality, $\mathcal{R} = 0.81 \pm 0.04 < 1$. The three-bin test successfully detects the nonclassicality of both the squeezed state and the phase-diffused state.

We further investigate the effects of the bin size and the bin distance on the nonclassicality certification. For the squeezed state, we find that the three-bin test works for a wide range of bin sizes [Fig. 2(d)], where $\sigma = 1.4$ is close to the optimum, showing $\mathcal{R} = 0.51 \pm 0.03 < 1$. The increase of \mathcal{R} for a large σ is due to a substantial coarse-graining effect, and for a small σ , the standard deviation of \mathcal{R} increases due to the limited number of counts collected in a single bin. For the phase-diffused squeezed state, we also find a similar behavior, as shown in Fig. 2(e). To investigate the bin distance effect, we perform the three-bin test by increasing the distance to $d = 3$ for the phase-diffused squeezed state, as shown in Fig. 2(c). In this case, $\mathcal{R} = 4.53 \pm 0.74 > 1$ for $\sigma = 1$, but we can again certify nonclassicality by decreasing σ [Fig. 2(f)], where even a larger deviation from the classical limit ($\mathcal{R} = 1$) is found compared with Fig. 2(e): $\mathcal{R} = 0.62 \pm 0.05 < 1$ at $\sigma = 0.5$. The three-bin test can detect nonclassicality with a wide range of σ without elaborate optimization.

IV. PERFORMANCE COMPARISON

Going beyond the demonstration of the three-bin test, we further highlight the advantages of using the coarse-graining method over the conventional moments method without coarse graining [21,22]. We consider a realistic nonclassicality certification scenario where only a finite number of samples by measurement are available. In the conventional

moment method, an $n \times n$ correlation matrix is constructed by up to n th order moments (for detailed explanations, refer to Appendix B). If its smallest eigenvalue is negative [$\lambda(n) < 0$], then the given state is nonclassical; in principle, this method can detect nonclassicality for any quantum state if a sufficiently large n with an infinite number of data is available [21]. In practice, however, because the number of data is finite, the standard deviation [$\delta\lambda(n)$] increases rapidly as n increases, which makes it difficult to attain sufficient statistical significance for nonclassicality certification. To quantitatively compare the statistical significances of the three-bin test (bin) and the moment method (moment), we introduce a violation degree \mathcal{V} , which is defined as the ratio between the distance from the classical limit and its standard deviation:

$$\mathcal{V}_{\text{bin}} = \frac{1 - \bar{\mathcal{R}}}{\delta\mathcal{R}}$$

$$\mathcal{V}_{\text{moment}}(n) = \frac{-\bar{\lambda}(n)}{\delta\lambda(n)}. \quad (4)$$

The upper bar and δ denote the mean value and the standard deviation, respectively. The classical limits of 1 and 0 have been used for \mathcal{R} and $\lambda(n)$, respectively. A positive (negative) \mathcal{V} shows detection (no detection) of nonclassicality, and the larger \mathcal{V} indicates the stronger statistical significance of nonclassicality certification.

Figure 3 compares the violation degrees of the two methods, \mathcal{V}_{bin} and $\mathcal{V}_{\text{moment}}$, tested for initial squeezing of (a) -1.6 ± 0.1 dB, (b) -2.3 ± 0.1 dB, and (c) -5.1 ± 0.1 dB. The moment method by $n = 2$ is equivalent to the variance criterion: $\mathcal{V}_{\text{moment}}(2) > 0$ leads to $\langle \delta\hat{x}^2 \rangle < 1$. One can find in

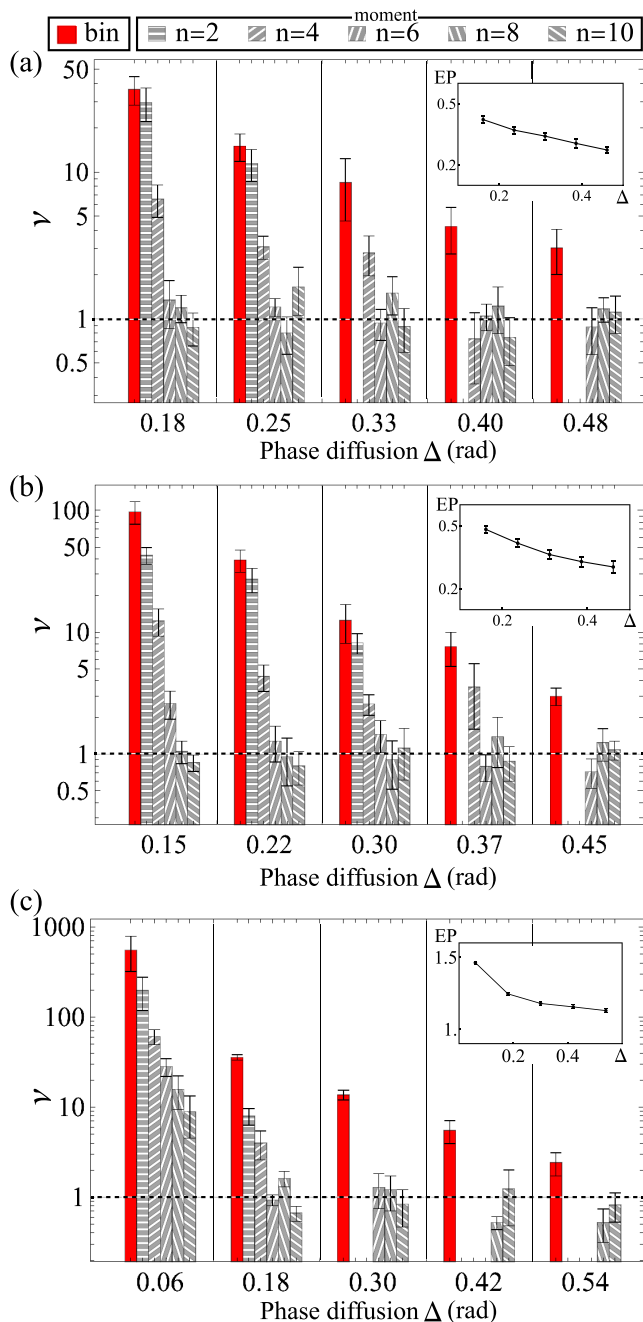


FIG. 3. Performance comparison between the three-bin test (bin) and the moment method (moment). In (a), the initial state has (\hat{x}, \hat{p}) quadrature variances of $(-1.6 \pm 0.1, 7.0 \pm 0.1)$ dB with $\Delta = 0.18 \pm 0.02$ rad, and in (b), the corresponding conditions are $(-2.3 \pm 0.1, 7.0 \pm 0.1)$ dB with $\Delta = 0.15 \pm 0.02$ rad. In (c), the initial state has (\hat{x}, \hat{p}) quadrature variances of $(-5.1 \pm 0.1, 10.6 \pm 0.1)$ dB with $\Delta = 0.06 \pm 0.06$ rad [33]. The violation degree \mathcal{V} quantifies the statistical significance of nonclassicality certification, as defined in Eq. (4). The horizontal dashed lines represent $\mathcal{V} = 1$, where the standard deviation is as large as the mean value to detect nonclassicality. When \mathcal{V} is negative (i.e., a failure of nonclassicality certification), the corresponding plot is omitted for clarity. Note that \mathcal{V} is plotted on a logarithmic scale. The three-bin test uses $d = 3$, and σ has been optimized to achieve the maximum \mathcal{V} . The insets plot the EP of the states under investigation. Error bars, representing one standard deviation, are obtained from five repeated experiments.

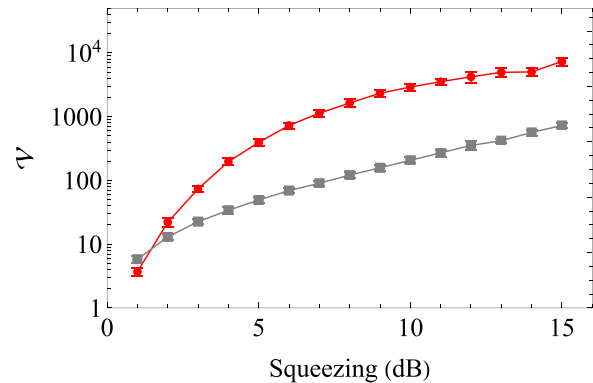


FIG. 4. Performance comparison between the three-bin test (red) and the variance test (gray) as increasing the \hat{x} -quadrature squeezing. Each point represents the violation degree (\mathcal{V}) by 1000 quadrature outcomes, which are generated by numerical simulations. We use the experimental conditions in Ref. [36] (phase diffusion: 1.7 mrad, optical loss: 2.5%) by considering squeezing up to 15 dB. \mathcal{V} is estimated by averaging 50 repeated simulations, where the error bar represents one standard deviation of the estimation. Note that \mathcal{V} is plotted on a logarithmic scale. The parameters used for the three-bin test are $d = 3$ and $\sigma = \sqrt{\delta \hat{x}^2}$. Lines serve as a visual guide.

Fig. 3 that, for a large phase diffusion, the moment method at $n = 2$ cannot detect nonclassicality [$\mathcal{V}_{\text{moment}}(2) < 0$, thus omitted in the figure], which agrees with the previous discussion for Fig. 1(c). Higher-order moments ($n \geq 4$) can detect the nonclassicality of such non-Gaussian states; however, for a larger n , due to the increased standard deviation $\delta \lambda(n)$, $\mathcal{V}_{\text{moment}}$ generally decreases as shown in Fig. 3. On the other hand, the three-bin test reliably detects nonclassicality in the entire range of phase diffusions, outperforming the moment method. The three-bin test generally becomes more powerful than the moment method for a larger phase diffusion.

We examine the operational significance of the phase-diffused squeezed states (naturally arising by optical propagation) as quantum resources. We place three insets in Fig. 3 to display the dynamics of the squeezed vacuum's entanglement potential [16] under phase diffusion, where we provide the detailed method to calculate entanglement potential in Appendix C. The entanglement potential of a quantum state quantifies the amount of quantum entanglement producible by injecting the quantum state through a passive beam splitter. Notably, such quantum entanglement is essential in multipartite quantum information tasks [34,35]. The insets exhibit that the entanglement potential remains positive under strong phase diffusions, which reveals the complex and robust nature of CV quantum resources beyond quantum squeezing.

Furthermore, the superiority of the three-bin test becomes even more pronounced with increasing squeezing. Figure 4 compares the violation degrees by the two methods, as obtained through numerical simulations. As the squeezing increases, the three-bin test outperforms the moment method even more significantly, showing the practicality of our method in the state-of-the-art experiment as well [36]. Note that for higher squeezing, coarse graining becomes a more critical issue because, with a finite number of bits available for analog-to-digital conversion, it becomes more challenging to

detect a broad range of signals required for quantum technologies [37–39] without losing the fine resolution for capturing the narrow structure of squeezing.

V. CONCLUSIONS

In conclusion, we have experimentally certified CV nonclassicality of both Gaussian and non-Gaussian states under coarse-grained measurement. Remarkably, we have found that—in the realistic case of a finite sample number—our coarse-grained measurement can outperform the conventional moments method based on fine-grained measurement [21,22], revealing the usefulness of coarse-grained measurement for a practical application to nonclassicality certification. This striking result is attributed to the facts that (i) for coarse-grained measurements, a large number of measurement outcomes are accumulated in the same bin, increasing the signal-to-noise ratio for probability estimation, and (ii) the three-bin test employed consists only of simple arithmetic, leaving little room for error propagation.

Our method employs coarse-grained data from single-quadrature measurement, which directly captures a phase-space structure narrower than the vacuum fluctuation, thereby showing no false detection of nonclassicality under coarse graining. We have tested the phase-diffused squeezed vacuum to compare the performances of the coarse-graining method and the conventional moments method. In the experiment, the coarse-graining method detected nonclassical states beyond the reach of the variance criterion, and more importantly, it outperformed the moments methods in the statistical significance with a finite number of samples. This advantage becomes more distinct for increasing squeezing and phase diffusion. It is remarkable because the coarse-graining method does not require fine-grained measurements and complex data processing. We have also addressed the operational relevance of the witnessed nonclassicality by examining the entanglement potential. Such nonclassicality can also be converted to quantum squeezing [40,41].

Our results strongly suggest that systematic and rigorous approaches to coarse-graining models may provide fundamental and practical tools in quantum information technologies [1–10,10–12]. We expect that our contributions will facilitate future studies to uncover the rich structure of CV quantum resources. For instance, it may be interesting to test quantum non-Gaussianity [42,43] with coarse-grained data, e.g., three bins, by using energy information [44,45] or more quadratures [46].

ACKNOWLEDGMENTS

This work was supported by the Ministry of Science and ICT (Grants No. NRF-2020M3E4A1080028, No. NRF-2022R1A2C2006179, and No. NRF-2019R1G1A1002337), and MSIT of Korea under the ITRC support program (Grant No. IITP-2023-2020-0-01606).

APPENDIX A: MEASURING THE PHASE DIFFUSION FROM HOMODYNE DATA

We explain how we jointly determine the initial squeezing parameter r , optical loss l , and phase diffusion Δ in the exper-

iment. The initial quantum state is a pure x -squeezed vacuum with variances of $\langle \delta \hat{x}_0^2 \rangle = e^{-2r}$ and $\langle \delta \hat{p}_0^2 \rangle = e^{2r}$, where $r > 0$. An optical loss is modeled as a beam-splitting interaction between a quantum state and a vacuum state with a reflectance of l . The phase diffusion is described as an incoherent mixing of phase rotation to a quantum state $\hat{\rho}$:

$$\hat{\rho} \mapsto \int_{-\infty}^{\infty} d\theta \frac{e^{-\theta^2/2\Delta^2}}{\sqrt{2\pi}\Delta} e^{i\hat{p}\theta} \hat{\rho} e^{-i\hat{p}\theta}, \quad (\text{A1})$$

where Δ determines the amount of phase diffusion. Let us investigate the variance of squeezing and antisqueezing quadrature, i.e., $\langle \delta \hat{x}^2 \rangle$ and $\langle \delta \hat{p}^2 \rangle$, for an x -squeezed vacuum under the presence of optical loss and phase noise. We obtain

$$\begin{aligned} \langle \delta \hat{x}^2 \rangle &= \int_{-\infty}^{\infty} d\theta \text{Var}(r, \theta, l) \frac{e^{-\theta^2/2\Delta^2}}{\sqrt{2\pi}\Delta} \\ &= l + (1-l)e^{-\Delta^2} (e^{-2r} \cosh \Delta^2 + e^{2r} \sinh \Delta^2), \end{aligned} \quad (\text{A2})$$

and

$$\begin{aligned} \langle \delta \hat{p}^2 \rangle &= \int_{-\infty}^{\infty} d\theta \text{Var}(r, \theta + \frac{\pi}{2}, l) \frac{e^{-\theta^2/2\Delta^2}}{\sqrt{2\pi}\Delta} \\ &= l + (1-l)e^{-\Delta^2} (e^{2r} \cosh \Delta^2 + e^{-2r} \sinh \Delta^2), \end{aligned} \quad (\text{A3})$$

where $\delta \hat{\delta} = \hat{\delta} - \langle \hat{\delta} \rangle$ denotes the deviation operator for $\hat{\delta}$, and $\text{Var}(r, \theta, l) = l + (1-l)(e^{-2r} \cos^2 \theta + e^{2r} \sin^2 \theta)$ is the variance of a rotated quadrature $\hat{x} \cos \theta + \hat{p} \sin \theta$ for the x -squeezed vacuum under the presence of optical loss only. Similarly, we derive the kurtosis K of the squeezing quadrature as

$$\begin{aligned} K &\equiv \frac{\langle (\delta \hat{x})^4 \rangle}{\langle (\delta \hat{x})^2 \rangle^2} = \frac{3}{\langle (\delta \hat{x})^2 \rangle^2} \int_{-\infty}^{\infty} d\theta [\text{Var}(r, \theta, l)]^2 \frac{e^{-\theta^2/2\Delta^2}}{\sqrt{2\pi}\Delta} \\ &= 3 + \frac{6(1-l)^2 e^{-4\Delta^2} \sinh^2(2\Delta^2) \sinh^2(2r)}{\langle (\delta \hat{x})^2 \rangle^2}, \end{aligned} \quad (\text{A4})$$

where we have used that kurtosis of a normal distribution is always three [47]. In the experiment, we obtain the variances $\langle (\delta \hat{x})^2 \rangle$ and $\langle (\delta \hat{p})^2 \rangle$, and the kurtosis K using the measured homodyne outcomes. We can then numerically calculate the squeezing parameter r , optical loss l , and phase diffusion amplitude Δ using Eqs. (A2)–(A4).

In the experiment, we collected 40 000 \hat{x} (squeezing) quadrature and \hat{p} (antisqueezing) quadrature data of each phase-diffused squeezed vacuum and generated 10 sets of 10 000 data using the bootstrap method. Following the procedure described in the previous paragraph, we obtained the initial squeezing r , the optical loss l , and the phase diffusion Δ . Figure 5 displays the estimated parameters as introducing an additional phase noise Δ_e . The estimated phase diffusion agrees well with the theoretical prediction $\Delta = \sqrt{\Delta_0^2 + \Delta_e^2}$, which can be derived from the fact that the variance of the sum of independent random variables is simply the sum of the variance of the random variables. The initial squeezing and the loss also behave as expected, exhibiting no changes due to the added noise.

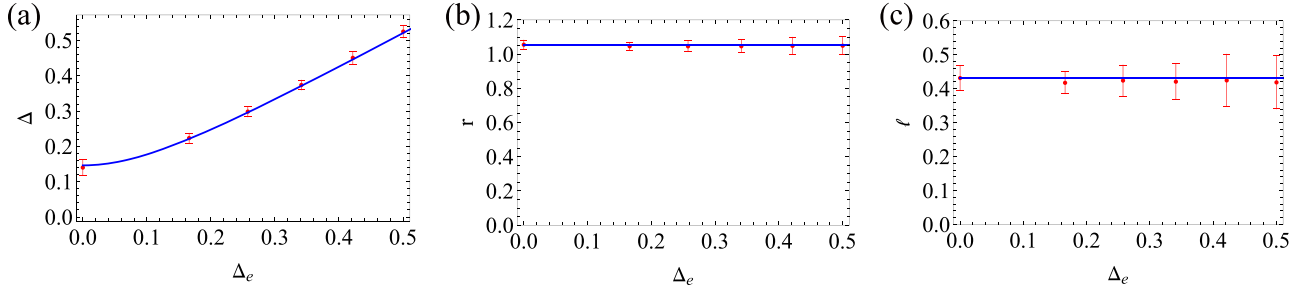


FIG. 5. Estimated parameters of the (a) phase diffusion Δ , (b) initial squeezing r , and (c) total optical loss l . Δ_e is the standard deviation of an added Gaussian phase noise. Red points are estimated parameters from quadrature data of the phase-diffused squeezed vacuum, and blue lines are expected theoretical values. Error bars are obtained by the bootstrap method.

APPENDIX B: NORMALLY ORDERED MOMENT METHOD FOR NONCLASSICALITY CERTIFICATION

The normally ordered moment method [21] employs an $n \times n$ matrix of normally order moments $\mathbf{M}(n)$ as

$$\mathbf{M}(n) = \begin{bmatrix} 1 & \langle : \hat{x} : \rangle & \cdots & \langle : \hat{x}^{n-1} : \rangle \\ \langle : \hat{x} : \rangle & \langle : \hat{x}^2 : \rangle & \cdots & \langle : \hat{x}^n : \rangle \\ \vdots & \vdots & \ddots & \vdots \\ \langle : \hat{x}^{n-1} : \rangle & \langle : \hat{x}^n : \rangle & \cdots & \langle : \hat{x}^{2n-2} : \rangle \end{bmatrix}, \quad (\text{B1})$$

where $\langle : \hat{x}^j : \rangle$ represents the normally ordered moment of the j th order. For any classical state, the matrix $\mathbf{M}(n)$ has no negative eigenvalue with all $n \in \{2, 3, 4, \dots\}$. Therefore, if there exists at least one negative eigenvalue of the matrix $\mathbf{M}(n)$ for some n , a given state is certified to be nonclassical. We note that the normally ordered moment $\langle : \hat{x}^j : \rangle$ can be rewritten as [48]

$$\langle : \hat{x}^j : \rangle = \frac{1}{2^{j/2}} \langle H_j(\hat{x}/\sqrt{2}) \rangle, \quad (\text{B2})$$

where $H_j(x)$ is the Hermite polynomial of the j th degree. It is straightforward to observe that the negative eigenvalue of $\mathbf{M}(2)$ detects the existence of squeezing. Furthermore, the eigenvalues of $\mathbf{M}(n)$ with $n \geq 3$ generally involve higher-order moments. This is why $\mathbf{M}(n)$ with $n \geq 3$ can detect nonclassical states without squeezing. To use the moment method for nonclassicality certification, the following sampling expression is used:

$$\langle : \hat{x}^j : \rangle \simeq \frac{1}{2^{j/2}N} \sum_{i=1}^N H_j(x_i/\sqrt{2}), \quad (\text{B3})$$

where x_i is the i th quadrature measurement, and N is the total number of data.

APPENDIX C: ENTANGLEMENT POTENTIAL OF PHASE-DIFFUSED SQUEEZED VACUUM

To determine whether the phase-diffused squeezed vacuum can produce quantum entanglement through a beam splitter, we calculate the entanglement potential (EP) [16] of the phase-diffused squeezed vacuum states that are cer-

tified in the experiment. We first reconstruct the density operator of the phase-diffused squeezed vacuum using the maximum-likelihood estimation method [49], which is based on quadrature measurement by rotating the quadrature angle. The reconstructed density operator is expressed as

$$\hat{\sigma} = \sum_{n=0}^{N_c} \sum_{m=0}^{N_c} \sigma_{nm} |n\rangle \langle m|, \quad (\text{C1})$$

where $|n\rangle$ is the n -photon Fock state, and N_c is the cutoff dimension. Here we choose $N_c = 10$ because the populations in the Fock basis are concentrated in low photon-number Fock states for the case of weakly squeezed vacuum. Then, we calculate the EP of the phase-diffused squeezed vacuum by using the following expression:

$$\text{EP}(\hat{\sigma}) = \log_2 \|\hat{\rho}_{\hat{\sigma}}^{T_A}\|, \quad (\text{C2})$$

where $\hat{\rho}_{\hat{\sigma}} = \hat{U}_{\text{BS}}(\hat{\sigma} \otimes |0\rangle \langle 0|) \hat{U}_{\text{BS}}^\dagger$ represents a two-mode quantum state generated by coherently mixing $\hat{\sigma}$ and vacuum $|0\rangle \langle 0|$ through a 50:50 beam splitter \hat{U}_{BS} :

$$\hat{\rho}_{\hat{\sigma}} = \sum_{n=0}^{N_c} \sum_{m=0}^{N_c} \sum_{j=0}^n \sum_{k=0}^m \sigma_{nm} \sqrt{\frac{1}{2^{n+m}} \binom{n}{j} \binom{m}{k}} |j\rangle \langle k| \otimes |n-j\rangle \langle m-k|, \quad (\text{C3})$$

and the superscript T_A denotes the partial transpose of the density operator, which yields

$$\hat{\rho}_{\hat{\sigma}}^{T_A} = \sum_{n=0}^{N_c} \sum_{m=0}^{N_c} \sum_{j=0}^n \sum_{k=0}^m \sigma_{nm} \sqrt{\frac{1}{2^{n+m}} \binom{n}{j} \binom{m}{k}} |j\rangle \langle k| \otimes |m-k\rangle \langle n-j|. \quad (\text{C4})$$

Here $\|\hat{\sigma}\| \equiv \text{tr} \sqrt{\hat{\sigma}^\dagger \hat{\sigma}}$ is the trace norm of the Hermitian operator $\hat{\sigma}$ which equals with the absolute sum of the eigenvalues for $\hat{\sigma}$. Therefore, we can compute EP in Eq. (C2) by solving the eigenvalue problem for the partially transposed density operator in Eq. (C4).

[1] M. V. Larsen, X. Guo, C. R. Breum, J. S. Neergaard-Nielsen, and U. L. Andersen, Deterministic generation

of a two-dimensional cluster state, *Science* **366**, 369 (2019).

- [2] W. Asavanant, Y. Shiozawa, S. Yokoyama, B. Charoensombutamon, H. Emura, R. N. Alexander, S. Takeda, J.-I. Yoshikawa, N. C. Menicucci, H. Yonezawa *et al.*, Generation of time-domain-multiplexed two-dimensional cluster state, *Science* **366**, 373 (2019).
- [3] Y.-S. Ra, A. Dufour, M. Walschaers, C. Jacquard, T. Michel, C. Fabre, and N. Treps, Non-Gaussian quantum states of a multimode light field, *Nat. Phys.* **16**, 144 (2020).
- [4] H.-S. Zhong, Y.-H. Deng, J. Qin, H. Wang, M.-C. Chen, L.-C. Peng, Y.-H. Luo, D. Wu, S.-Q. Gong, H. Su *et al.*, Phase-programmable Gaussian boson sampling using stimulated squeezed light, *Phys. Rev. Lett.* **127**, 180502 (2021).
- [5] L. S. Madsen, F. Laudenbach, M. F. Askarani, F. Rortais, T. Vincent, J. F. F. Bulmer, F. M. Miatto, L. Neuhaus, L. G. Helt, M. J. Collins *et al.*, Quantum computational advantage with a programmable photonic processor, *Nature (London)* **606**, 75 (2022).
- [6] O. Pfister, Continuous-variable quantum computing in the quantum optical frequency comb, *J. Phys. B: At. Mol. Opt. Phys.* **53**, 012001 (2020).
- [7] Y. Zhang, Z. Chen, S. Pirandola, X. Wang, C. Zhou, B. Chu, Y. Zhao, B. Xu, S. Yu, and H. Guo, Long-distance continuous-variable quantum key distribution over 202.81 km of fiber, *Phys. Rev. Lett.* **125**, 010502 (2020).
- [8] O. Kovalenko, Y.-S. Ra, Y. Cai, V. C. Usenko, C. Fabre, N. Treps, and R. Filip, Frequency-multiplexed entanglement for continuous-variable quantum key distribution, *Photon. Res.* **9**, 2351 (2021).
- [9] X. Guo, C. R. Breum, J. Borregaard, S. Izumi, M. V. Larsen, T. Gehring, M. Christandl, J. S. Neergaard-Nielsen, and U. L. Andersen, Distributed quantum sensing in a continuous-variable entangled network, *Nat. Phys.* **16**, 281 (2020).
- [10] J. A. H. Nielsen, J. S. Neergaard-Nielsen, T. Gehring, and U. L. Andersen, Deterministic quantum phase estimation beyond N00N states, *Phys. Rev. Lett.* **130**, 123603 (2023).
- [11] C. Oh, C. Lee, C. Rockstuhl, H. Jeong, J. Kim, H. Nha, and S.-Y. Lee, Optimal Gaussian measurements for phase estimation in single-mode Gaussian metrology, *npj Quantum Inf.* **5**, 10 (2019).
- [12] I. Derkach, V. C. Usenko, and R. Filip, Squeezing-enhanced quantum key distribution over atmospheric channels, *New J. Phys.* **22**, 053006 (2020).
- [13] D. Gottesman, A. Kitaev, and J. Preskill, Encoding a qubit in an oscillator, *Phys. Rev. A* **64**, 012310 (2001).
- [14] T. Kouadou, F. Sansavini, M. Ansquer, J. Henaff, N. Treps, and V. Parigi, Spectrally shaped and pulse-by-pulse multiplexed multimode squeezed states of light, *APL Photon.* **8**, 086113 (2023).
- [15] M. S. Kim, W. Son, V. Bužek, and P. L. Knight, Entanglement by a beam splitter: Nonclassicality as a prerequisite for entanglement, *Phys. Rev. A* **65**, 032323 (2002).
- [16] J. K. Asbóth, J. Calsamiglia, and H. Ritsch, Computable measure of nonclassicality for light, *Phys. Rev. Lett.* **94**, 173602 (2005).
- [17] G. M. D'Ariano, C. Macchiavello, and M. G. A. Paris, Detection of the density matrix through optical homodyne tomography without filtered back projection, *Phys. Rev. A* **50**, 4298 (1994).
- [18] A. I. Lvovsky and M. G. Raymer, Continuous-variable optical quantum-state tomography, *Rev. Mod. Phys.* **81**, 299 (2009).
- [19] N. Biagi, M. Bohmann, E. Agudelo, M. Bellini, and A. Zavatta, Experimental certification of nonclassicality via phase-space inequalities, *Phys. Rev. Lett.* **126**, 023605 (2021).
- [20] U. L. Andersen, T. Gehring, C. Marquardt, and G. Leuchs, 30 years of squeezed light generation, *Phys. Scr.* **91**, 053001 (2016).
- [21] G. S. Agarwal, Nonclassical characteristics of the marginals for the radiation field, *Opt. Commun.* **95**, 109 (1993).
- [22] E. V. Shchukin and W. Vogel, Nonclassical moments and their measurement, *Phys. Rev. A* **72**, 043808 (2005).
- [23] W. Vogel, Nonclassical states: An observable criterion, *Phys. Rev. Lett.* **84**, 1849 (2000).
- [24] T. Kiesel, W. Vogel, B. Hage, J. DiGuglielmo, A. Sambrowski, and R. Schnabel, Experimental test of nonclassicality criteria for phase-diffused squeezed states, *Phys. Rev. A* **79**, 022122 (2009).
- [25] J. Schneeloch, P. B. Dixon, G. A. Howland, C. J. Broadbent, and J. C. Howell, Violation of continuous-variable Einstein-Podolsky-Rosen steering with discrete measurements, *Phys. Rev. Lett.* **110**, 130407 (2013).
- [26] D. S. Tasca, Ł. Rudnicki, R. M. Gomes, F. Toscano, and S. P. Walborn, Reliable entanglement detection under coarse-grained measurements, *Phys. Rev. Lett.* **110**, 210502 (2013).
- [27] J. Park, S.-W. Ji, J. Lee, and H. Nha, Gaussian states under coarse-grained continuous variable measurements, *Phys. Rev. A* **89**, 042102 (2014).
- [28] J. Kofler and Č. Brukner, Classical world arising out of quantum physics under the restriction of coarse-grained measurements, *Phys. Rev. Lett.* **99**, 180403 (2007).
- [29] C. Gabriel, C. Wittmann, D. Sych, R. Dong, W. Mauerer, U. L. Andersen, C. Marquardt, and G. Leuchs, A generator for unique quantum random numbers based on vacuum states, *Nat. Photon.* **4**, 711 (2010).
- [30] S. Raeisi, P. Sekatski, and C. Simon, Coarse graining makes it hard to see micro-macro entanglement, *Phys. Rev. Lett.* **107**, 250401 (2011).
- [31] J. Park, J. Lee, and H. Nha, Verifying single-mode nonclassicality beyond negativity in phase space, *Phys. Rev. Res.* **3**, 043116 (2021).
- [32] Y. Cai, J. Roslund, G. Ferrini, F. Arzani, X. Xu, C. Fabre, and N. Treps, Multimode entanglement in reconfigurable graph states using optical frequency combs, *Nat. Commun.* **8**, 15645 (2017).
- [33] To obtain the data for Fig. 3(c), we perform an experiment with a CW optical parametric oscillator, which is similar to the one in *Opt. Lett.* **34**, 1060 (2009).
- [34] B. Hage, A. Sambrowski, J. DiGuglielmo, A. Franzen, J. Fiurášek, and R. Schnabel, Preparation of distilled and purified continuous-variable entangled states, *Nat. Phys.* **4**, 915 (2008).
- [35] P. van Loock and S. L. Braunstein, Multipartite entanglement for continuous variables: A quantum teleportation network, *Phys. Rev. Lett.* **84**, 3482 (2000).
- [36] H. Vahlbruch, M. Mehmet, K. Danzmann, and R. Schnabel, Detection of 15 dB squeezed states of light and their application for the absolute calibration of photoelectric quantum efficiency, *Phys. Rev. Lett.* **117**, 110801 (2016).
- [37] M. Tse, H. Yu, N. Kijbunchoo, A. Fernandez-Galiana, P. Dupej, L. Barsotti, C. D. Blair, D. D. Brown, S. E. Dwyer, A. Effler *et al.*, Quantum-enhanced advanced LIGO detectors in the era of gravitational-wave astronomy, *Phys. Rev. Lett.* **123**, 231107 (2019); F. Acernese, M. Agathos, L. Aiello, A. Allocca, A.

- Amato, S. Ansoldi, S. Antier, M. Arne, N. Arnaud, S. Ascenzi *et al.*, Increasing the astrophysical reach of the advanced Virgo detector via the application of squeezed vacuum states of light, *ibid.* **123**, 231108 (2019).
- [38] T. Michel, J. Y. Haw, D. G. Marangon, O. Thearle, G. Vallone, P. Villoresi, P. K. Lam, and S. M. Assad, Real-time source-independent quantum random-number generator with squeezed states, *Phys. Rev. Appl.* **12**, 034017 (2019).
- [39] L. S. Madsen, V. C. Usenko, M. Lassen, R. Filip, and U. L. Andersen, Continuous variable quantum key distribution with modulated entangled states, *Nat. Commun.* **3**, 1083 (2012).
- [40] B. Hage, A. Franzen, J. DiGuglielmo, P. Marek, J. Fiurášek, and R. Schnabel, On the distillation and purification of phase-diffused squeezed states, *New J. Phys.* **9**, 227 (2007).
- [41] R. Filip, Distillation of quantum squeezing, *Phys. Rev. A* **88**, 063837 (2013).
- [42] R. Filip and L. Mišta, Jr., Detecting quantum states with a positive Wigner function beyond mixtures of Gaussian states, *Phys. Rev. Lett.* **106**, 200401 (2011).
- [43] L. Lachman and R. Filip, Quantum non-Gaussianity of light and atoms, *Prog. Quantum Electron.* **83**, 100395 (2022).
- [44] M. G. Genoni, M. L. Palma, T. Tufarelli, S. Olivares, M. S. Kim, and M. G. A. Paris, Detecting quantum non-Gaussianity via the Wigner function, *Phys. Rev. A* **87**, 062104 (2013).
- [45] C. Hughes, M. G. Genoni, T. Tufarelli, M. G. A. Paris, and M. S. Kim, Quantum non-Gaussianity witnesses in phase space, *Phys. Rev. A* **90**, 013810 (2014).
- [46] L. Happ, M. A. Efremov, H. Nha, and W. P. Schleich, Sufficient condition for a quantum state to be genuinely quantum non-Gaussian, *New J. Phys.* **20**, 023046 (2018).
- [47] H. Cramér, *Mathematical Methods of Statistics* (PMS-9) (Princeton University Press, Princeton, 1946).
- [48] A. Wünsche, Ordered operator expansions and reconstruction from ordered moments, *J. Opt. B: Quantum Semiclass. Opt.* **1**, 264 (1999).
- [49] A. I. Lvovsky, Iterative maximum-likelihood reconstruction in quantum homodyne tomography, *J. Opt. B: Quantum Semiclass. Opt.* **6**, S556 (2004).